Vol. 37 No. 9 SCIENCE IN CHINA (Series A) September 1994

Theoretical and Experimental Researches of Post-microbuckling for Fiber-reinforced Composites*

WEI Yue-Guang (魏悦广),

(*Institute of Mechanics, Academia Sinica, Beijing* 100080, *PRC*)

YANG Wei (杨 卫) and HUANG Ke-Zhi (HWANG Keh-Chih 黄克智)

(*Tsinghua University, Beijing* 100084, *PRC*)

Received January 25, 1994.

Abstract Post-microbuckling is a fundamental feature of compressive failure process for the unidirectional-fiber-reinforced composites and laminated composites. The post-microbuckling behavior of composites under compression in the light of the Kevlar49-reinforced 648/BF3.400 (brittle epoxy) and EP (flexible epoxy) is studied, theoretically and experimentally. Analytical results of compressive strength are in good agreement with experimental results, qualitatively and quantitatively. By the experimental research, the post-microbuckling feature of the advancing kink band model is clearly displayed.

Keywords: elastic-plastic instability, post-microbuckling, kink band.

Studies of compressive failure on fiber-reinforced composites are of a wide practical significance. But for three decades, some fundamental facts are still unclear, e. g. what is the limit for which the Rosen[1] formula is suitable? what is the main reason for the large difference in the compressive strengths between results from the Rosen formulas and from experiment? It is well known that the compressive strengths of typical composites predicted using the Rosen formulas are far larger than those obtained in experiments[2].

Following the deducing process of the Rosen formulas, we think that the Rosen formula of a shear model is only suitable for the composite with a weak strength matrix and weak interface, while that of an extension model is only suitable for the composite with a loose fiber distribution ($V_f<0.1$, V_f is the volume fraction of fiber) or/and with high-strength fibers.

Argon[3] and Fleck and Budiansky[2] considered the plastic deformation of matrix when fiber composite was compressed in the fiber direction, and their formulas of compressive strength were too sensitive to the initial curvature of fibers. Piggott and Harris[4] carried out a systematic experimental research on compressive failure for various fiber-reinforced composites, and they concluded that from small to medium densities of fibers ($0.05<V_f<0.31$), the compressive failure models are from laminating to kinking.

* Project supported by the National Natural Science Foundation of China.

Steif[5,6] *first applied the bifurcation theory* developed by Hill and Hutchinson[7] to the study of laminated composites which were simulated by hyperelastic ones. An eigenvalue problem of elastic-plastic bifurcation for laminated composites was solved accurately by Wei and Yang[8]: the compressive failure of unidirectional composites is mainly due to the plastic bifurcation of fibers, and from this conclusion they obtained the compressive strengths which are in excellent agreement with the experimental results given in Refs. [4, 9]. Yang and Wei[10] first analysed the mechanism of the kink band and the compressive buckle band[10] and they performed post-microbuckling analyses with a bridging kink band model[11]. They calculated the bridging force using Hutchinson's bifurcation model of column[12], and obtained the overall compressive stress-strain relation using the conservative law of J integral.

Based on Ref. [11], in this paper the compressive kinking failure of two Kevlar49-reinforced kinds of epoxy is studied by detailed division of the region of material parameters, and the overall compressive stress strain curves are theoretically investigated. For comparison, material parameters and the behavior of compressive microbuckling are determined and studied experimentally. The composite specimens are Kevlar49-reinforced 648/BF3.400 and EP.

1 Bridging Model of Post-microbuckling

Post-microbuckling is featured by the bridging fibers which suddenly lose the matrix constraint at the critical instability stress σ_{fc} following the precursor of matrix damage. This feature can be represented by the kink band bridging model shown in Fig. 1[11]. The bridging force of fibers in the kink band is calculated by adopting Hutchinson's plastic bifurcation model of column shown in the insert of Fig. 1. S is the distance between the geometrical center and the instantaneous rotation center in the cross section (See Ref. [11] for detail). In the following calculation, fibers and matrices will be treated as bilinear materials and linear elastic materials, respectively. The relations between bridging force σ_{fB}, rotation angle θ of column, S and vertical

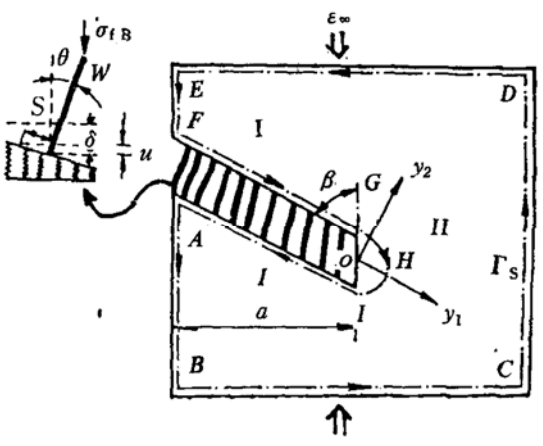

Fig. 1. Bridging model by kink band and J-integral contour.

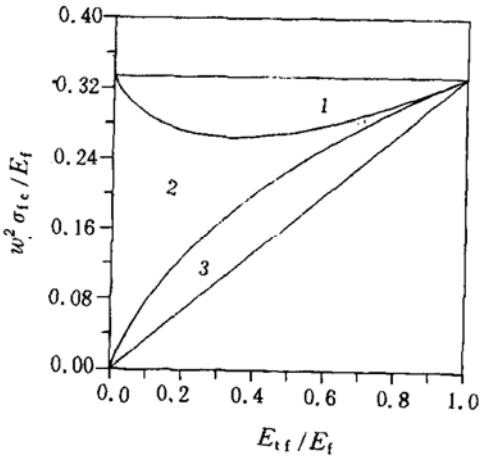

Fig. 2. The regions of S monotonically increasing (S-I) and decreasing (S-D). 1; S-D zone; 2, S-I zone; 3, S-D zone.

displacement δ on the top of the column can be determined from the geometry and balance relations[11].

The strength and flexibility of fiber-reinforced composites after losing instability can be characterized by S alone[11]. The initial values of S and $\frac{dS}{d\theta}$ dominate the features of the post-microbuckling.

When S is monotonically increasing (hereinafter referred to as S-I), the following relations are easily derived[11]:

$$\begin{cases} \dfrac{\sigma_B}{\sigma_C} = 1 - \dfrac{1}{4w\hat{\sigma}_{fc}}[(1-s)^2 - t(1+s)^2]\sin\theta, \\ S = 2\sqrt{1+2w\lambda\tan\theta+w^2\tan^2\theta}\,\cos\left(\psi - \dfrac{2\pi}{3}\right) - w\tan\theta, \\ \psi = \dfrac{1}{3}\arccos\left\{ \dfrac{-\left|\dfrac{\omega\hat{\sigma}_{fc}}{2\cos\theta} - (1+w\tan\theta)^3 - (\lambda-1)(1+3w^2\tan^2\theta)\right|}{(1+2w\lambda\tan\theta+w^2\tan^2\theta)^{3/2}} \right\}, \\ \dfrac{\delta}{2h_f} = s\sin\theta + w(1-\cos\theta) + w\varepsilon_c, \end{cases} \tag{1}$$

where

$$\hat{\sigma}_{fc} = \frac{\sigma_{fc}}{E_f}, \quad \sigma_B = \sigma_{fB}V_f\sin\beta, \quad \sigma_C = \sigma_{fc}V_f\sin\beta, \quad \sigma_{fc} = E_f\varepsilon_1 + E_{tf}(\varepsilon_c - \varepsilon_1),$$

$$\varepsilon_1 = \frac{\sigma_0}{E_f}, \quad t = \frac{E_{tf}}{E_f}, \quad \lambda = \frac{1+t}{1-t}, \quad s = \frac{S}{h_f}, \quad \omega = \frac{12w^2}{1-t}, \tag{2}$$

$w = W/h_f$, $2w$ is the width of kink band, $2h_f$ is the thickness of fiber layer, ε_1 is the yielding strain of fiber, σ_C and σ_B may be interpreted as the averaged instability stress and the bridging stress along the inclined kink band with an inclination angle β, E_f is the fiber Young's modulus, and E_{tf} is the linear hardening modulus.

When S is monotonically decreasing (hereinafter referred to as S-D), we have[11]

$$\begin{aligned} \frac{\sigma_B}{\sigma_C} &= 1 - \frac{3w}{w\hat{\sigma}_{fc}}\left\{\sin\theta[1 - 2\lambda s_0 + s_0^2 - 2(\lambda - s_0)\xi + \xi^2] + \int_0^\xi \sin\theta\tan\theta\left(\frac{d\theta}{d\xi}\right)^{-1}d\xi\right\} \\ &= \frac{\cos\theta}{\omega\hat{\sigma}_{fc}}\left\{2\lambda - 3s_0 + s_0^3 - 3(1-s_0^2)\xi + 3s_0\xi^2 + \xi^3 \right. \\ &\qquad \left. + \frac{1}{\sin\theta}\int_0^\xi \left[3(s_0+\xi) + \tan\theta\left(\frac{d\theta}{d\xi}\right)^{-1}\right]\sin\theta\left(\frac{d\theta}{d\xi}\right)^{-1}d\xi\right\}, \end{aligned} \tag{3}$$

where

$$\xi = s - s_0. \tag{4}$$

The Formula of $\frac{\delta}{2h_f}$ is the same as the fourth equation of Eq. (1), and $s_0 = S_0/h_f$ is the initial value of s.

From Eq. (1) or/and Eq. (3), s_0 can be specified by ω, λ, $\hat{\sigma}_{fc}$:

$$s_0 = 2\cos\left(\psi_0 - \frac{2\pi}{3}\right),\ \psi_0 = \frac{1}{3}\arccos\left(-\left|\frac{\omega}{2}\hat{\sigma}_{fc} - \lambda\right|\right), \tag{5}$$

and whether S is monotonically increasing or decreasing can be judged by the following equation:

$$s_0 - \frac{1-\sqrt{t}}{1+\sqrt{t}} \begin{cases} <0 & \text{(increasing);} \\ >0 & \text{(decreasing).} \end{cases} \tag{6}$$

In Eq. (1) or Eq. (3), there are three variables: σ_B, θ, s. If s is taken as an argument and σ_B and θ are seen as the functions of s, then $\delta/2h_f$ can be obtained from the fourth formula of Eq. (1). Especially, the solutions of Eq. (3) are somewhat difficult to obtain. This equation is first transformed into a higher-order quasilinear differential equation on θ. Since the initial (boundary) values $\theta(s_0)$ and s_0 are known from Eq. (5) and experiment of Kevlar49/epoxy, the numerical solution can be obtained by the well-established Runge-Kutta method.

It is convenient to plot the divisional figure of S-I and S-D in a parameter plane. The relations of initial material parameters formulated by Eqs. (5) and (6) are expressed concisely in Fig. 2.

2 Bridging Toughening

Following the formulation by Yang and Wei[10], the toughness increment by fiber bridging across the kink band could be measured in terms of J integral, defined by

$$J = \int_\Gamma \left(U dy_2 - T_i \frac{\partial u_i}{\partial y_1}\, dl\right), \tag{7}$$

where $U = \int_0^{\varepsilon_{ij}} \sigma_{km}\, d\varepsilon_{km}$ is the strain energy density, and T_i and u_i represent the traction and displacement vectors, respectively. The index notation of tensor is adopted here, in a coordinate system $y_1 - y_2$ aligned with the kink band, as shown in Fig. 1. Summation convention for repeated indices is implied. The contour Γ for the J integral is outlined in Fig. 1 which follows the marked points $ABCDEFGHIA$.

2.1 *The Case of Monotonically Decreasing S*

In this case, the continuous increase of the bridging stress σ_B would justify the endured loading within the composite during the kink band growth, an assumption essential to validating the path independency of J integral. When evaluated along the closed contour Γ, the loop integral vanishes, and one obtains

$$J_\infty = J_{tip} + J_B, \tag{8}$$

where J_∞ represents the J integral evaluated counterclockwise along the exterior loop *ABCDEF* (Γ_∞), and J_{tip} denotes J integral evaluated counterclockwise along the inner loop IHG. The latter signifies the driving force for the kink band growth. J_B in Eq. (8) denotes the toughness increment by fiber bridging.

2.2 *The Case of Monotonically Increasing S*

The case of *S*-I would result in gradual declination of the bridging stress σ_B/σ_C. The elastic unloading which inevitably occurs in this case would decimate the path independency of J integral. However, from the conservation of energy we have

$$J_\infty = \int_{\Gamma_\infty} \left\{ U_e dy_2 - T_i \frac{\partial u_i}{\partial y_1} dl \right\} - \sin\beta \frac{\partial}{\partial a} \int_A (\hat{U} - U_e) dA = J_{tip} + J_B, \tag{9}$$

where

$$U_e = \frac{1}{2} C_{ijkl}(\varepsilon_{ij} - \varepsilon^*_{ij})(\varepsilon_{kl} - \varepsilon^*_{kl}) = \frac{1}{2} \sigma_{ij}(\varepsilon_{ij} - \varepsilon^*_{ij}). \tag{10}$$

The significance of U_e can be explained as an elastic strain energy density for the composite which has a stress-free initial strain ε^*_{ij}. Eq. (10) can also be taken as the definition of ε^*_{ij}. C_{ijkl} in Eq. (10) denotes the elastic tensor of the fiber-reinforced composite. $\hat{U}$ is the historical dependent deformational energy received in the composite cell. For the case of *S*-I, under uniform compression, the formation of kink band would produce elastic unloading from the pre-bifurcation strain level ε_c over all the composite cells. Therefore, ε^*_{ij} can be assumed to take constant value at any material points passed by the kink band.

2.3 *Toughening Ratio*

The calculations of J_{tip} and J_B are conducted by the following formulas:

$$J_{tip} = (1 - V_f) E_m \varepsilon_c (W\varepsilon_c + \varepsilon_t) \sin\beta, \tag{11}$$

where

$$\frac{\delta_t}{h_f} = \frac{w E_f V_f}{E_m (1 - V_f)} [(1-t)(2 - \varepsilon_1/\varepsilon_c)\varepsilon_1 + t\varepsilon_c], \tag{12}$$

$$J_B = \int_0^\delta \sigma_B d\delta, \tag{13}$$

where E_m is the Young's modulus of matrix, and σ_B is the bridging stress which are formulated in Eq. (1) for *S*-I and in Eq. (3) for *S*-D.

The toughening value J_∞/J_{tip} can be calculated from Eqs. (8) (or (9)), (11) and (13).

3 Overall Compressive Stress Strain Curves

The overall compressive stress-strain curves σ_∞-ε_∞ can be assessed from Eq. (8) when the remote J integral (J_∞) is known. The stress-strain distribution along the outer contour Γ_∞ (Fig. 1) can be approximately treated as in the unidirectional stress state[13]. The calculations for J_∞ can be conducted consecutively for the cases of *S*-I and *S*-D. The final results are

$$\frac{J_\infty}{J_{tip}} = \begin{cases} Z_1/Z_2, & (S\text{-D}); \\ \{Z_1-(F_b^{-1}-1)(E-E_t)(\varepsilon_c-\varepsilon_I)^2\}/Z_2, & (S\text{-I}), \end{cases} \tag{14}$$

where

$$\begin{cases} Z_1=\left(\Sigma_1+E_t\varepsilon_I+\dfrac{\delta}{4W}E_tF_b\right)\dfrac{\delta}{W}+\Sigma_1(2\varepsilon_I-\varepsilon_1)+E_t\varepsilon_I^2, \\ Z_2=(1-V_f)\left(\varepsilon_c+\dfrac{\delta_t}{W}\right)\varepsilon_cE_m, \end{cases} \tag{15}$$

$$\varepsilon_\infty=\varepsilon_{II}\approx\varepsilon_I+\frac{\delta}{2W}F_b=\begin{cases} \{V_f(\sigma_{fc}/\sigma_C)\sigma_B-\Sigma_1\}/E_t+\dfrac{\delta}{2W}F_b & (S\text{-D}), \\ \{V_f(\sigma_{fc}/\sigma_C)\sigma_B-\sigma_C\}/E+\varepsilon_c+\dfrac{\delta}{2W}F_b & (S\text{-I}); \end{cases} \tag{16}$$

$$\sigma_\infty=\frac{a}{B}\sigma_I+\left(1-\frac{a}{B}\right)\sigma_{II}=V_f\frac{\sigma_{fc}}{\sigma_C}\frac{a}{B}\sigma_B+\left(1-\frac{a}{B}\right)(\Sigma_1+E_t\varepsilon_\infty); \tag{17}$$

$$\begin{cases} E=E_fV_f+E_m(1-V_f), \\ E_t=E_{tf}V_f+E_m(1-V_f), \\ \Sigma_1=(E_f-E_{tf})V_f\varepsilon_1, \end{cases} \tag{18}$$

where the variables and parameters with the subscripts I and II are corresponding to the regions I and II shown in Fig. 1, respectively, B and H are the width and height of material cells shown in Fig. 1, $F_b=2W/H$ characterizes the area fraction on the free surface, σ_B and δ are computed from Eq. (1) or (3).

The σ_∞-ε_∞ curves can be given by cancelling J_∞/J_{tip} and F_b from the expressions of Eqs. (8) (or (9)), (14), (16) and (17). The overall compressive stress-strain curves of the Kevlar49-reinforced flexible epoxy (EP) and brittle epoxy (648/BF3.400) are shown in Fig. 3(a) and (b), respectively. During calculations, we take $w=5.5$, $\varepsilon_1=0.01$, $E_f/E_m=34.4$ for the case of brittle matrix (*S*-D), and $w=3$, $\varepsilon_1=0.018$, $E_f/E_m=49.6$ for the case of flexible matrix (*S*-I), and $\varepsilon_c/\varepsilon_1=1.5$, $V_f=0.4$ for all cases. These parameter

values come from experiments to be discussed in the next section. The cases of *S*-I and *S*-D are plotted in Fig. 3(a) and (b), respectively. The three curves in Fig. 3 are corresponding to three hardening moduli t. For comparison, experimental curves are plotted in Fig. 4. By comparing Fig. 3(a) and (b) with Fig. 4(a) and (b), respectively, theoretical and experimental results are very conformable.

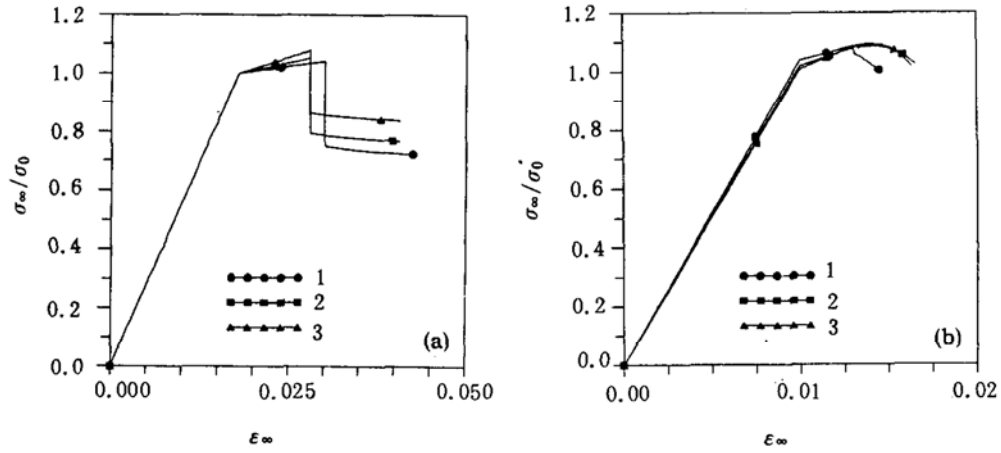

Fig. 3. The theoretical results of overall compressive stress strain curves. (a) Corresponding to Kevlar49/EP. $\alpha/\beta=0.4$; 1, $t=0.0167$; 2, $t=0.0500$; 3, $t=0.1000$. (b) Corresponding to Kevlar49/(648/BF3.400). $\alpha/\beta=0.4$; 1, $t=0.10$; 2, $t=0.15$; 3, $t=0.20$.

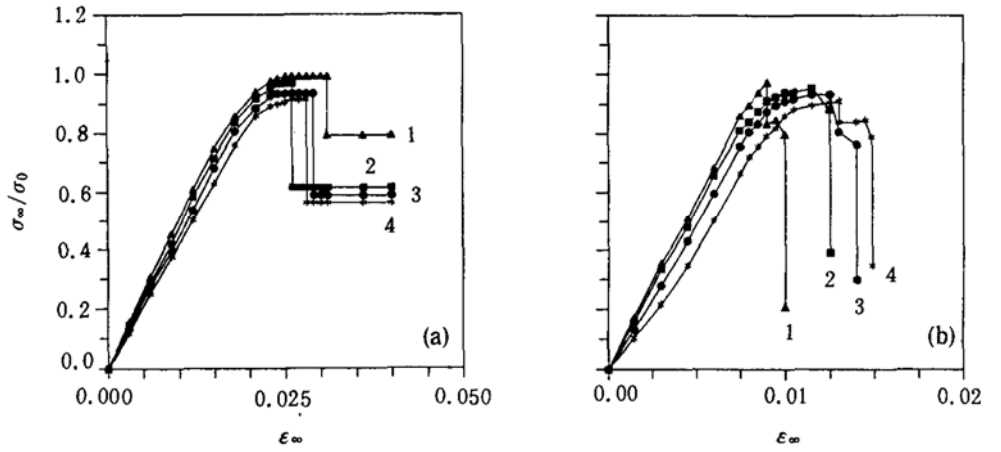

Fig. 4. The experimental results of overall compressive stress strain curves. (a) corresponding to Kevlar49/EP, (b) corresponding to Kevlar49/(648/BF3.400). 1, A; 2, B; 3, C; 4, Sp. D. $\sigma_0=250$ MPa.

4 Compressive Experiments on Kevlar49/Epoxy

In this section, we will discuss experimental researches of Kevlar49-reinforced 648/BF3.400 (brittle epoxy) and EP (flexible epoxy). The qualities of the composites are shown in Table 1.

Table 1 Known Qualities of Fiber and Matrix Materials

Composite	Tensile strength (GPa)	Tensile modulus (GPa)	Limit strain (%)
Kevlar49	3.4	124	2.3
648/BF3.4000		3.6	0.78
EP		2.5	3.0

In order to investigate the action of surface defects on the formation of kink bands and to study the behavior of the buckle-driven lamination, each specimen was manufactured with a set of cracks (three cracks) near the free surface. The lengths of cracks become smaller from the outside to the interior of specimens, from l_1 to l_3. The specimen numbers with different sets of cracks are given in Table 2. The geometrical size of each specimen is 30 mm × 7 mm × 12 mm.

Table 2 The Specimen Numbers and Crack Lengths l_i (mm)

Specimen	A	B	C	D
l_1	0	6	8	10
l_2	0	4	6	8
l_3	0	2	4	6

The overall stress and strain curves of Kevlar49-reinforced 648/BF3.400 and EP from experiment are shown in Fig. 4 (b) and (a), respectively. The experimental results verify the analytical evaluations. The kinking patterns on the side surface of specimens are shown in Fig. 5, where (a) and (b) correspond to the cases of flexibleepoxy matrices, and the postmicrobuckling is the advance of kink band till passing through the specimen section; (c) corresponds to the case of brittle epoxy matrix, and the postmicrobuckling is from kinking to laminating.

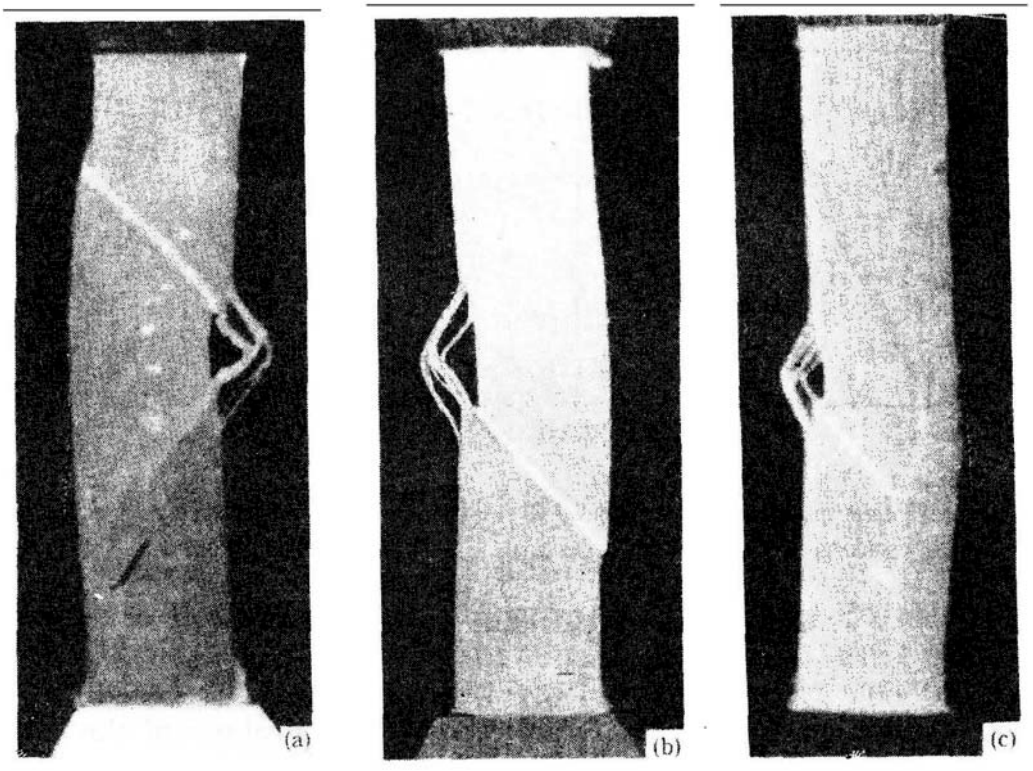

Fig. 5. Kink bands on the side surface of a specimen. (a) and (b) for the flexible matrices EP. (c) for the brittle matrix 648/BF3.400.

Figure 6 gives magnification figures of kink band for the specimens with flexible matrix: (a) is a complete picture of a kink band;(b) displays the local magnification of a kink band; (a) and (b) ,correspond to specimen B and specimen C in Table 2,

respectively; (c) is double kink bands simultaneously formed in specimen A (without surface cracks).

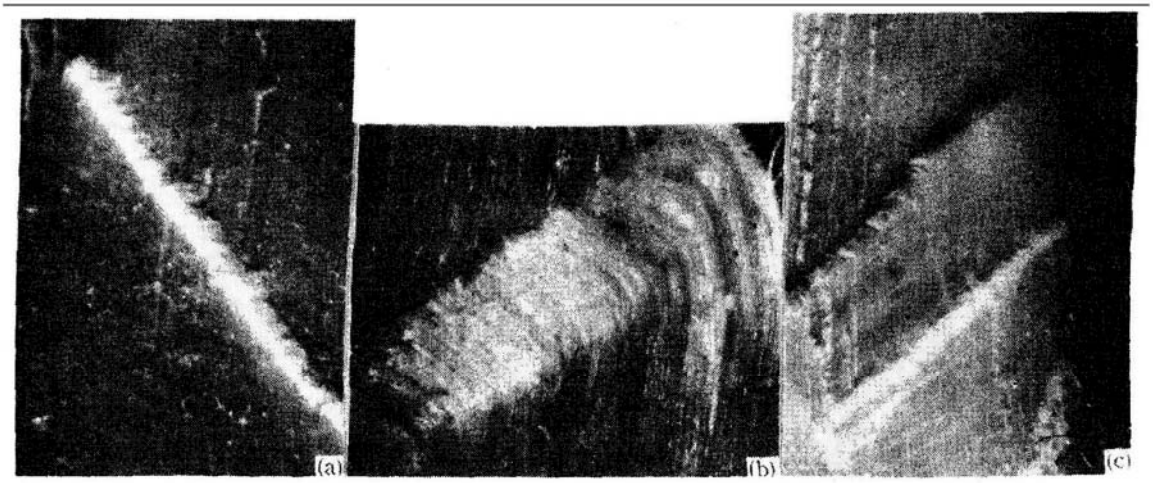

Fig. 6. Magnification of kink band. (a) (×12.6) and (b) (×49) , Kink band is produced with surface cracks in advance in the specimen; (c) (×12.6), two kink bands are formed simultaneously without surface cracks.

To facilitate the inspection and measurement on kink band, we pre-sticked the moire of 40-line/mm on a side surface of some specimens, so that the complete picture of kink band could be observed and measured with microscope (PM-6 Olympus). When a specimen is compressed, the moire is deformed with the specimen under strain. Especially, the kink band features can be displayed and registered by the moire. A complete picture of a kink band on the side surface of the specimen is given in Fig. 7. The widths of the kink band can be measured from this figure. The widths of the growing kink band (thin) and the penetrating kink band (thick) are $2W=0.75-1.0$ mm and $2W=0.25-0.4$ mm, respectively. The ratios $w\,(=W/h_f)$ of the growing kink band and penetrating kink band can be found out, respectively, $w=2-3$ and $6-8$ from the known fiber layer width $2h_f=0.125$ mm. The volume fraction of fiber $V_f=0.4$.

5 Conclusions

1. The mechanical qualities of post-microbuckling of fiber-reinforced composites are mainly dominated by the kink band geometry and the plastic kinking of bridging fibers. The overall mechanical feature of composites can be predicted effectively by adopting the column plastic bifurcation model.

2. The compressive failure formation of composites is sensitive to surface defects and the brittleness and flexibility of matrix.

3. Compared with previous researches on the compressive failure of composites, our investigation goes much deeper theoretically and obtains conformable theoretical and experimental results.

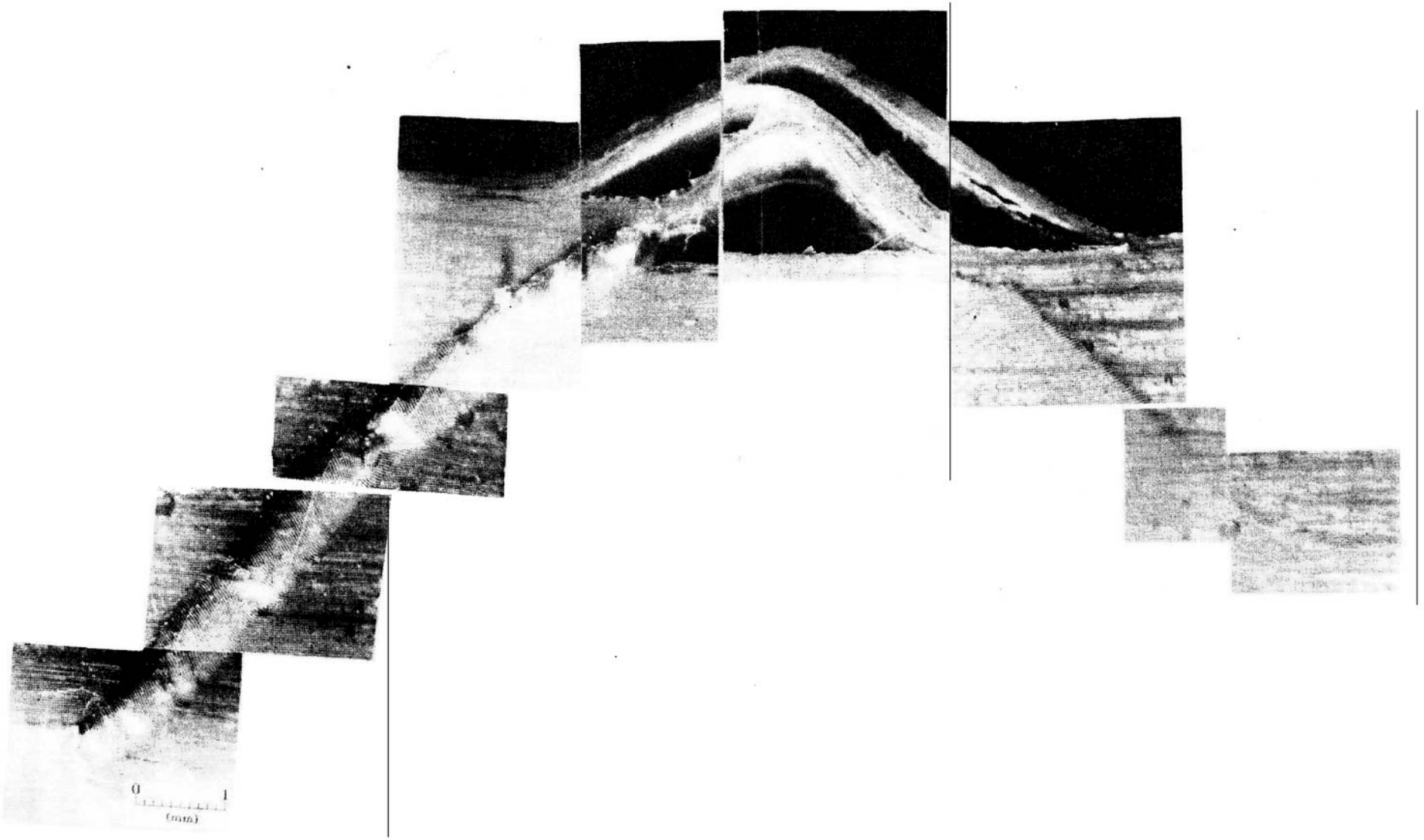

Fig. 7. Magnified kink bands on the overall side surface of a specimen.

References

1 Rosen, B. W., *Fiber Composite Materials. Am. Soc. Metals Seminar*, 1965, Metals Park, Ohio, Chapter 3.

2 Fleck, N. A. & Budiansky, B., in *Proc. IUTAM Symp. on Inelastic Deformation of Composite Materials*, Troy, New York, 29 May, 1990.

3 Argon, A. S., *Treatise of Materials Science and Technology*, Vol. 1, Academic Press, New York, 1972, p.79.

4 Piggott, M. R. & Harris, B., *J. Mater. Sci.*, 1980, **15**, 2523.

5 Steif, P. S., *Int. J. Solids Structs.*, 1990, **26**:549.

6 Steif, P. S., *Int. J. Solids Structs.*, 1987, **23**:1235.

7 Hill, R. & Hutchinson, J. W., *J. Mech. Phys. Solids*, 1975, **23**:238.

8 Wei, Y. G. & Yang, W., *Acta Aero. et Astro. Sinica* (in Chinese), 1992, **A13**(7):A388.

9 Kulkarni, S. V., Rice, J. S. & Rosen, B. W., *NASA-CR*-112334, 1973.

10 Yang, W. & Wei, Y. G., *Int. J. Damage Mechanics*, 1992, **1**(1):80.

11 Wei, Y. G. & Yang, W., *Acta Mechanica Sinica*, 1993, **9**(1):33.

12 Hutchinson, J. W., *J. Mech. Phys. Solids*, 1973, **21**:163.

13 Budiansky, B. & Amazigo, C., *J. Mech. Phys. Solids*, 1989, **37**:93.